Hyperpolarized Magnetic Resonance and Ligand Binding

Lecture Notes

Benno Meier

January 6, 2025

Colophon
This document was typeset with the help of KOMA-Script and LaTeX using the kaobook class.
The source code of this book's template is available at:
https://github.com/fmarotta/kaobook

Contents

Introduction

These notes accompany a set of lectures on Hyperpolarized NMR spectroscopy and ligand-binding that are given as part of the practical course 5145 - Advanced Chemical Biology.

A significant fraction of the material is advanced and can be skipped in a first reading. These sections are marked with an asterisk (*), and are not relevant for any examinations that take place within course 5145.

The lectures are structured as follows:

- In chapter 1 - `The Signal and the Noise`, we will discuss the source of the NMR signal which is the nuclear spin polarization.
- In chapter 2 - `Relaxation`, we will see how the spin polarization attains its thermal equilibrium value through the process of relaxation.
- In chapter 3 - `Hyperpolarization`, we will see how a process called dynamic nuclear polarization (DNP) can be used to generate spin polarization that is orders of magnitude larger than the thermal equilibrium nuclear spin polarization.
- In chapter 4 - `Ligand-binding`, we will see how NMR can be used to study the binding of small molecules (ligands) to large molecules (proteins), and how hyperpolarization may accelerate this process.

1 The Signal and the Noise

1.1 The Main Ideas

The objective of hyperpolarization is to increase the sensitivity of magnetic resonance by polarizing or aligning the spins to a degree that is *above* its thermal equilibrium value.

In this lecture we will first learn how to calculate the nuclear and electron spin polarization using the Boltzmann distribution. For experts in magnetic resonance, we will then calculate the same quantity using the spin density matrix. Knowledge of the polarization enables us to calculate the magnetization. The precessing magnetization gives rise to a voltage in the NMR coil, and this voltage is called the signal.

The polarization is by no means the only factor that determines the sensitivity of magnetic resonance. Indeed, a state of hyperpolarization can often be achieved only at the expense of analyte concentration or throughput, which adversely affects sensitivity.

In this lecture, we will learn

- how to calculate the polarization at thermal equilibrium
- how to calculate the magnetization for a given polarization
- how to calculate the induced voltage in the RF coil
- how to calculate the Signal-to-Noise Ratio (SNR) per unit time.

1.2 The Polarization

The term describes the "net" alignment of spins in NMR and EPR. Since only the aligned spins give rise to the NMR signal, the signal is directly proportional to the polarization. This lecture series is about "Hyper-Polarization", that is about achieving a state of "higher than normal" polarization. As we will see soon, the potential to do so is huge.

1.2.1 The Nuclear Zeeman Interaction

In both the EPR and the NMR spin systems that we will discuss in this lecture the coupling between the spin and the external magnetic field is the dominant interaction. This coupling is called . For a classic magnetic moment we have

$$E = -\boldsymbol{\mu}\mathbf{B}. \tag{1.1}$$

Nuclear magnetic resonance is based on the fact that many nuclei have both a magnetic moment $\boldsymbol{\mu}$, and an angular momentum $\boldsymbol{J}$. The two quantities are parallel vectors, and we write

$$\boldsymbol{\mu} = \gamma \boldsymbol{J}. \tag{1.2}$$

Herein γ is the gyromagnetic ratio, a quantity that depends on the nucleus. $\boldsymbol{J}$ is an angular momentum operator. In magnetic resonance, we prefer to work with *dimensionless* angular momentum poperators $\boldsymbol{I}$ with

$$\hbar \boldsymbol{I} = \boldsymbol{J}. \tag{1.3}$$

$\boldsymbol{I}$ is a vector of operators, i.e. $\boldsymbol{I} = (\hat{I}_x, \hat{I}_y, \hat{I}_z)$.

Much like earth's magnetic field aligns the magnetic moment of a compass needle,[1] a magnetic field tends to align nuclear spins.

1: Note that without friction the compass needle would oscillate about the earth's field indefinitely, just like a swing without friction would swing indefinitely about earth's gravitational field. Also in NMR we need friction processes to achieve alignment, and these are known as T_1 processes.

The energy of the interaction, using Equations (1) and (2) is

$$E = -\boldsymbol{\mu} \boldsymbol{B} \tag{1.4}$$

Now we choose to apply the magnetic field along the z-axis, i.e. $\boldsymbol{B} = (0, 0, B_0)$, and we obtain

$$E = -\gamma \hbar \hat{I}_z B_0 \tag{1.5}$$

Note that the above equation does not give a value (in Joule), but rather it specifies an operator. The operator that describes the energy structure of the system is called the Hamiltonian in quantum mechanics, and written, in this case, as

$$\mathscr{H} = -\gamma \hat{I}_z B_0, \tag{1.6}$$

Note that we have dropped $\hbar$ - we follow the usual convention in NMR and express energies as angular frequencies. In NMR we deal with systems with discrete energy levels, and the spin operators can be represented as matrices. The eigenvectors of the Hamiltonian matrix correspond to the stationary states of the system, and the eigenvalues to their respective energies.

1.2.2 Spin states and matrix representation*

In order to find the energy values, we need to find the eigenvalues of $\hat{I}_z$. To do so, we have to calculate the *matrix representation* of $\hat{I}_z$. This can only be done with respect to a defined basis. We denote the spin states with

$$\left|I, m_{-1/2}\right\rangle = |1/2, -1/2\rangle = |-1/2\rangle = |-\rangle = |\beta\rangle \tag{1.7}$$
$$\left|I, m_{+1/2}\right\rangle = |1/2, 1/2\rangle = |1/2\rangle = |+\rangle = |\alpha\rangle \tag{1.8}$$

The spin states form an orthonormal basis. This means that

$$\langle\alpha|\alpha\rangle = \langle\beta|\beta\rangle = 1. \tag{1.9}$$
$$\langle\alpha|\beta\rangle = \langle\beta|\alpha\rangle = 0. \tag{1.10}$$

Note that the above expression describe the orthogonality of (normalized) eigenvectors with respect to the scalar product.

The notation $|I, m\rangle$ is the general notation for a Ket for a single spin. With the symbol $|1/2, -1/2\rangle$, we have simply inserted the value for a spin $1/2$ in the $-1/2$ state. There are nuclei with higher spin. For example, deuterium has total spin $I = 1$, and to give its eigenstate with $m_z = 0$, we would write $|1, 0\rangle$. Note that m_z takes values $-I, -I + 1, ..., I$, so that for a spin one nucleus like deuterium we have three eigenstates.

Recall from quantum mechanics that $\hat{I}_z$ extracts the projection quantum number m_z.

The matrix representation of $\hat{I}_z$ for a single spin-1/2 particle is

$$\begin{pmatrix} \langle\alpha|\hat{I}_z|\alpha\rangle & \langle\alpha|\hat{I}_z|\beta\rangle \\ \langle\beta|\hat{I}_z|\alpha\rangle & \langle\beta|\hat{I}_z|\beta\rangle \end{pmatrix} = \begin{pmatrix} 1/2 & 0 \\ 0 & -1/2 \end{pmatrix} \tag{1.11}$$

We see that $\hat{I}_z$ is already diagonal, with eigenvalues $1/2$ and $-1/2$.

1.2.3 Energy levels of a single nuclear spin

The energy levels of the spin are the eigenvalues of the Hamiltonian. These in turn are the eigenvalues of $\hat{I}_Z 4$, multiplied by γB_0:

$$E = \pm\frac{1}{2}\gamma B_0. \tag{1.12}$$

We see that the splitting between the two states depends on the nuclear gyromagnetic ratio γ and is proportional the magnetic field B_0.

Note that the nuclear Zeeman interaction by itself is *isotropic*, i.e. the splitting does not depend on the orientation of the magnetic field.

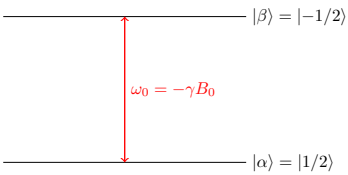

Figure 1.1: Spitting of Zeeman levels in an external magnetic field. The figure is correct for nuclei with a positive gyromagnetic ratio, for which the Larmor frequency is negative. These are, for example ^{1}H, ^{13}C, ^{14}N, but not ^{15}N, which has a negative gyromagnetic ratio.

The electron Zeeman interaction*

As we will see in more detail soon, the electron Zeeman interaction depends on the orientation of the magnetic field with respect to the so-called g-tensor. For the purpose of calculating polarizations, we can ignore this dependence, and use the free electron g-factor as an approximation, i.e. $g \approx 2.0023$. The gyromagnetic ratio of a free electron is $\gamma_S = g\mu_B$, where μ_B is the Bohr magneton.

Note that the anisotropy of the electron Zeeman interaction is analogous to the chemical shift anisotropy in NMR, but it may be of the order of unity, where as chemical shifts in NMR are specified in ppm.

1.2.4 The Boltzmann Distribution

The polarization P of the spins is defined as follows

$$P = \frac{p_{|\alpha\rangle} - p_{|\beta\rangle}}{p_{|\alpha\rangle} + p_{|\beta\rangle}} = p_{|\alpha\rangle} - p_{|\beta\rangle} = 1 - 2p_{|\beta\rangle} \tag{1.13}$$

Herein, $p_{|\alpha\rangle}$ and $p_{|\beta\rangle}$ are the fractions of spins in the $|\alpha\rangle$ and $|\beta\rangle$ states respectively. Note that all spins are either in the $|\alpha\rangle$ or in the $|\beta\rangle$ state, i.e. $p_{|\alpha\rangle} + p_{|\beta\rangle} = 1$.

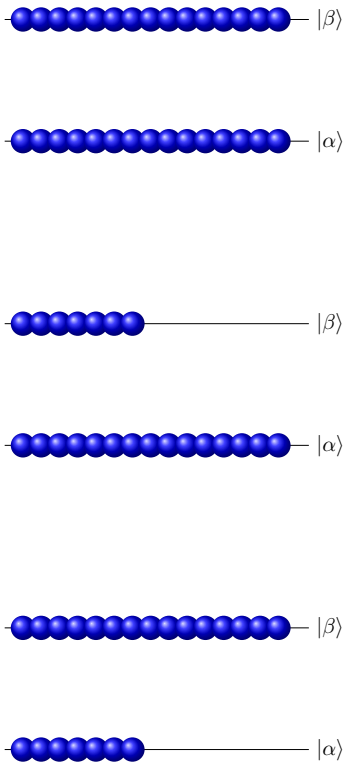

Figure 1.2: Spin state populations corresponding to zero polarization (top), positive hyperpolarization (middle), and negative hyperpolarization (bottom).

We have not treated relaxation, and so we have no mechanism which would cause a spin to transition, e.g., from $|\alpha\rangle$ to $|\beta\rangle$. Nevertheless, we know that spin systems (usually) achieve a thermal equilibrium. In doing so, they exchange energy with their surrounding, which is called the *lattice*. The time constant for this process is the *spin-lattice* relaxation time constant T_1. After a few T_1s, the system achieves equilibrium with the lattice, and the ratio of the populations is then given by

$$\frac{p_{|\beta\rangle}}{p_{|\alpha\rangle}} = \exp\left(-\frac{\hbar\gamma B}{kT}\right) \tag{1.14}$$

where T is the lattice (e.g. sample) temperature.

Solving the above equation for $p_{|\beta\rangle}$ gives

$$p_{|\beta\rangle} = (1 - p_{|\beta\rangle}) \exp\left(-\frac{\hbar\gamma B}{kT}\right) \tag{1.15}$$

$$p_{|\beta\rangle}\left(1 + \exp\left(-\frac{\hbar\gamma B}{kT}\right)\right) = \exp\left(-\frac{\hbar\gamma B}{kT}\right) \tag{1.16}$$

$$p_{|\beta\rangle} = \frac{\exp\left(-\frac{\hbar\gamma B}{kT}\right)}{1 + \exp\left(-\frac{\hbar\gamma B}{kT}\right)} \tag{1.17}$$

$$= \frac{1}{1 + \exp\left(+\frac{\hbar\gamma B}{kT}\right)} \tag{1.18}$$

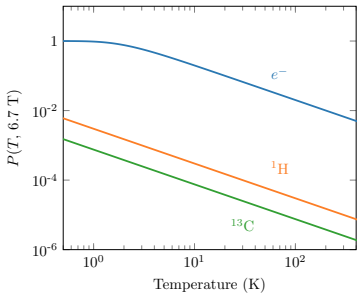

Figure 1.3: Thermal equilibrium polarization for the electron (blue), ^{1}H (orange) and ^{13}C at a field of 6.7 Tesla

Insertion into Eq. (1.13), and using the relation $\tanh(x) = 1 - \frac{2}{1+\exp(2x)}$ yields

$$P = 1 - 2p_{|\beta\rangle} = 1 - \frac{2}{1 + \exp\left(+\frac{2\hbar\gamma B}{2kT}\right)} = \tanh\left(\frac{\hbar\gamma B}{2kT}\right), \tag{1.19}$$

With this expression we can calculate the thermal equilibrium polarization for any spin 1/2 nucleus, as well as the electron for any field and temperature. The result is shown in Fig. 3.1 for a magnetic field of 6.7 Tesla. Note the exceedingly small polarization of the nuclear spins at ambient temperature (approximately 10^{-5} at 300 Kelvin). The electron has a much larger gyromagnetic ratio, and a correspondingly higher polarization. At temperatures of the order of 1 Kelvin, electron spins become fully polarized.

[1]: Overhauser (1953), 'Polarization of Nuclei in Metals'

[2]: Carver et al. (1953), 'Polarization of Nuclear Spins in Metals'

Albert Overhauser realised in 1952 [1], that in metals the large polarization of conduction electrons could be transfered to nuclear spins by saturating the electron spin transition. Charlie Slichter thought Al's prediction to be correct, and, together with his student Tom Carver, conceived and conducted an experiment that showed a dramatic increase in the NMR signal intensity of ^{7}Li in lithium metal. They published their work in August 1953 [2], only months after Overhauser had published his ideas.

An inspiring account of the "birth of hyperpolarization" has been

given by Slichter [3].

Since Overhauser's discovery, several other hyperpolarization mechanisms have been discovered, one of them () also by Carver. However, the term dynamic nuclear polarization was taken, and is reserverd for hyperpolarization mechanisms in which *electrons* are the source of hyperpolarization.

[3]: Slichter (2010), 'The Discovery and Demonstration of Dynamic Nuclear Polarization-A Personal and Historical Account'

Equation (1.19) suggests a straight forward way to achieve near unity polarization, namely to apply a field of a few Tesla, and cool the sample down to Millikelvin temperatures. This approach has actually been explored and is called brute-force hyperpolarization [4]. The major problem with brute-force polarization is that spin-lattice relaxation becomes exceedingly long at temperatures below 1 K, and a state of high polarization may not be achieved at all. The relaxation time may be shortened using paramagnetic dopants, but the polarization levels achieved in this way are still lower than what can be achieved with DNP.

[4]: Hirsch et al. (2015), 'Brute-Force Hyperpolarization for NMR and MRI'

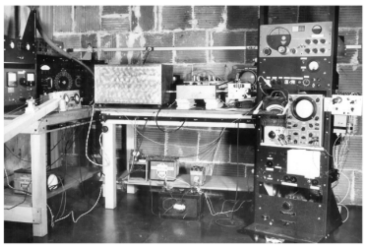

Figure 1.4: The first DNP Spectrometer. Reproduced from Ref. [3]

Under ambient conditions, we have $\hbar\gamma B \ll kT$, or $x \ll 1$. We may then use the expansion $\tanh(x) \approx x$, and the polarization for a spin 1/2 evaluates to[2]

$$P \approx \frac{\hbar\gamma B}{2kT}. \tag{1.20}$$

This is the high-temperature approximation in NMR. It applies for all spin 1/2 nuclei at practical fields (< 100 Tesla) and temperatures (> 1 Kelvin), but not for electron spins at 1 Kelvin and 5 Tesla.

1.2.5 Polarization and the Density Matrix*

We conclude this section by discussing the polarization for spins > 1/2. In principle, one can use (1.14) to solve also for a higher spin. There is however a more elegant way which is part of the standard NMR toolbox. Namely we will calculate the expectation value of $\hat{I}_z$. For a fully polarized spin system we have $P = 1$, and the expecation value of $\hat{I}_z$ equals 1/2. For a system with full negative polarization, the exepectation value equals $-1/2$.

We define the polarization for an arbitrary spin I as

$$P = \frac{1}{I}\left\langle \hat{I}_z \right\rangle \tag{1.21}$$

The polarization defined in this way assumes values from -1 to $+1$ for any spin I. It should be noted however that for spins > 1/2, this definition has to be used with care. Consider, as an example an ensemble of ^{14}N spins, which are all in the $|1;0\rangle$ state. Although this is a highly-ordered, pure state, it has no magnetization, and the above definition ascribes it zero polarization.

The expectation value of an operator can be calculated using the *density*

operator. The thermal equilibrium density operator is written as

$$\hat{\rho} = \frac{1}{Z}\exp\left(-\frac{\hbar\mathscr{H}}{kT}\right) = \frac{1}{Z}\exp\left(+\frac{\hbar\gamma\hat{I}_z B_0}{kT}\right) \tag{1.22}$$

Herein, Z is the partition sum,

$$Z = \sum_j \exp(-E_j/kT) = \sum_{m_z=-I}^{I} \exp(+\hbar\gamma B m_z/kT) \tag{1.23}$$

$$= \sum_{m_z=-I}^{I} \exp(\tilde{B}m_z), \tag{1.24}$$

where we have introduced the dimensionless quantity $\tilde{B} = \hbar\gamma B/kT$ to shorten the notation.

We choose the Zeeman basis in which the Hamiltonian is diagonal. Therefore, the matrix representation of $\hat{\rho}$ is also diagonal, with entries $\exp\left(\tilde{B}m_z\right)$. To calculate the expectation value of $\hat{I}_z$, we have to calculate the trace over $\hat{\rho}\hat{I}_z$. For a spin-1/2 we have

$$\begin{aligned}
P &= \frac{1}{\frac{1}{2}}\mathrm{Tr}\left(\hat{\rho}\hat{I}_z\right) = \frac{2}{Z}\mathrm{Tr}\left(\begin{pmatrix}\exp(\tilde{B}\cdot(1/2)) & 0\\ 0 & \exp(\tilde{B}\cdot(-1/2))\end{pmatrix}\begin{pmatrix}1/2 & 0\\ 0 & -1/2\end{pmatrix}\right)\\
&= \frac{\exp(\tilde{B}\cdot(1/2)) - \exp(-\tilde{B}\cdot(1/2))}{\exp(-\tilde{B}\cdot(1/2)) + \exp(\tilde{B}(1/2))}\\
&= \frac{\exp(\tilde{B}\cdot(1/2)) + \exp(-\tilde{B}\cdot(1/2)) - 2\exp(-\tilde{B}\cdot(1/2))}{\exp(-\tilde{B}\cdot(1/2)) + \exp(+\tilde{B}(1/2))}\\
&= 1 - \frac{2\exp(-\tilde{B}\cdot(1/2))}{\exp(-\tilde{B}\cdot(1/2)) + \exp(+\tilde{B}(1/2))}\\
&= 1 - \frac{2}{1+\exp(\tilde{B})} = 1 - \frac{2}{1+\exp(2\tilde{B}/2)} = \tanh(\tilde{B}/2)
\end{aligned}$$

which is the familiar result.

For a spin 1 we get, in complete analogy,

$$\begin{aligned}
P &= \frac{1}{1}\mathrm{Tr}\left(\hat{\rho}\hat{I}_z\right)\\
&= \frac{1}{Z}\mathrm{Tr}\left(\begin{pmatrix}\exp(-\tilde{B}) & 0 & 0\\ 0 & \exp(0) & 0\\ 0 & 0 & \exp(+\tilde{B})\end{pmatrix}\begin{pmatrix}1 & 0 & 0\\ 0 & 0 & 0\\ 0 & 0 & -1\end{pmatrix}\right)\\
&= \frac{\sum_{m=-1}^{1} m_z \exp(\tilde{B}m_z)}{\sum_{m=-I}^{I}\exp(\tilde{B}m_z)}
\end{aligned}$$

For an arbitrary spin, the polarization is

$$P = \frac{1}{I}\frac{\sum_{m=-I}^{I} m_z \exp(\tilde{B}m_z)}{\sum_{m=-I}^{I}\exp(\tilde{B}m_z)} \tag{1.25}$$

We can use the above expression to derive a simple expression for the polarization of a nucleus with *arbitrary spin I* in the high-temperature

limit, using the expansion $\exp(x) \approx 1 + x$. Then we have

$$P \approx \frac{1}{I} \frac{\sum_{m=-I}^{I} m_z(1 + \tilde{B} m_z)}{\sum_{m=-I}^{I} 1 + x} \tag{1.26}$$

In the nominator the sum over m_z is zero, and in the denominator we can ignore x. Then, using the relation

$$\sum_{m=-I}^{I} m^2 = \frac{I(I+1)(2I+1)}{3} \tag{1.27}$$

we have

$$P \approx \frac{1}{I} \frac{\tilde{B} \sum_{m=-I}^{I} m_z^2}{(2I+1)} = \frac{1}{I} \frac{\tilde{B} I(I+1)(2I+1)}{3(2I+1)} = \frac{\tilde{B}(I+1)}{3} \tag{1.28}$$

Note that this expression corresponds to (1.20) for a spin $I = 1/2$.

1.3 The Magnetization

The polarization is a so-called *intensive* qunatity. It does not change when we incraese the amount of sample in our detector. The NMR signal of course is an *extensive* quantity, it does scale with the number of spins in the detector.

The NMR signal is induced in a coil by the precessing magnetization. The magnetization is usually defined as magnetic moment per unit volume, with the unit A/m. The magnetic moment is the expectation value of $\boldsymbol{\mu}$, and we denote the spin density (the number of spins N per volume V) with $n = N/V$. Then we have

$$M = n \langle \mu \rangle = n\gamma\hbar \langle \boldsymbol{I} \rangle . \tag{1.29}$$

We assume that the magnetic field is again applied along the z axis.[3] Then, there will be only a magnetization along z, given by

$$M_z = n\gamma\hbar \left\langle \hat{I}_z \right\rangle = n\gamma\hbar \mathrm{Tr}(\hat{\rho}\hat{I}_z) \tag{1.30}$$

Now we have already calculated the expectation value of $\hat{I}_z$, and we may write it as $\left\langle \hat{I}_z \right\rangle = IP$, where P is given by Eq. (1.25).

The general result for the magnetization is therefore

$$M_z = n\gamma\hbar IP, \tag{1.31}$$

where P is given by equation (1.25).

In the case of a spin 1/2 in the high-field limit this may be written, using equation (1.19), as

$$M_z = n\gamma\hbar \frac{1}{2} \tanh(\tilde{B}/2). \tag{1.32}$$

In the case of an arbitrary spin in the high-temperature limit we use

3: A radio-frequency (RF) pulse is of course requried to generate the transverse magnetization that gives rise to the NMR signal. We assume that the RF pulse is a perfect 90 degree pulse, so that the transverse magnetization *after* the pulse will equal the longitudinal magnetization M_z *before* the pulse.

(1.28), and have

$$M_z = n\gamma\hbar I\frac{\tilde{B}(I+1)}{3} = \frac{n\gamma^2\hbar^2 BI(I+1)}{3kT} \tag{1.33}$$

This equation is known as the Curie law.

1.4 The NMR Signal

While it is difficult to make accurate predictions for signal intensities (and signal-to-noise ratio) from first principles, it is straightforward to estimate the order of magnitude of these quantities.

1.4.1 The induced voltage

Following a 90 degree or $\pi/2$ - pulse, the magnetization will precess about the magnetic field with a frequency ω. Faraday's law of induction states that the voltage induced in a coil with N turns by a changing flux Φ is

$$V_S = -N\frac{\mathrm{d}\Phi}{\mathrm{d}t}. \tag{1.34}$$

The flux is given as the magnetic field B flowing through the coil, multiplied with its cross-section A. The magnetic field in turn is given by $B = \mu_0 M$. If we assume M to precess according to $M = M_z \sin(\omega t)$, we have

$$V_S = -NA\mu_0\omega M_z \cos(\omega t) \tag{1.35}$$

The induced signal scales as $\gamma^3 B_0^2$. We might be tempted to use lots of turns to achieve a larger voltage. However, the coil geometry also dictates the noise level.

The Principle of Reciprocity*

An alternative way to estimate the voltage has been given by Hoult in his now classic paper [5]. Clearly, if a given current generates a larger magnetic field at a certain point in space, then a precessing magnetic moment at that point will induce a larger voltage in the same coil. This is the principle of reciprocity.

[5]: Hoult et al. (1976), 'The Signal-To-Noise Ratio of the Nuclear Magnetic Resonance Experiment'

To derive the principle of reciprocity we need the Biot-Savart Law, which gives the magnetic field produced by a current I running along a wire C. We assume the current to be constant, and rewrite the law for later convenience:

$$\boldsymbol{B}_1(\boldsymbol{r}) = \frac{\mu_0}{4\pi}\int_C \frac{I\mathrm{d}\boldsymbol{l}\times\boldsymbol{r}}{r^3} = -I\frac{\mu_0}{4\pi}\int_C \frac{\boldsymbol{r}\times\mathrm{d}\boldsymbol{l}}{r^3} \tag{1.36}$$

We furthermore need the vector potential of a magnetic dipole,

$$\boldsymbol{A}(\boldsymbol{r}') = \frac{\mu_0}{4\pi}\frac{\boldsymbol{m}\times\boldsymbol{r}'}{r'^3}, \tag{1.37}$$

and the fact that the magnetic field due to $\boldsymbol{A}$ is given by

$$\boldsymbol{B}(\boldsymbol{r}) = \mathrm{rot}\boldsymbol{A}. \tag{1.38}$$

Now we use Faraday's law of induction

$$V = -\frac{\mathrm{d}\Phi}{\mathrm{d}t} = -\frac{\mathrm{d}}{\mathrm{d}t}\iint_{\mathrm{Area}} \boldsymbol{B}\cdot\mathrm{d}\boldsymbol{a}, \tag{1.39}$$

where $\mathrm{d}\boldsymbol{a}$ is the surface element. Now we insert Equation (1.38), use Stokes' theorem, insert the expression for $\boldsymbol{A}$, and rearange using the cyclic relation $(\boldsymbol{a}\times\boldsymbol{b})\cdot\boldsymbol{c} = (\boldsymbol{b}\times\boldsymbol{c})\cdot\boldsymbol{a}$:

$$V = -\frac{\mathrm{d}}{\mathrm{d}t}\iint_{\mathrm{Area}} \mathrm{rot}\boldsymbol{A}\cdot\mathrm{d}\boldsymbol{a} = -\frac{\mathrm{d}}{\mathrm{d}t}\int_C \boldsymbol{A}\cdot\mathrm{d}\boldsymbol{l} \tag{1.40}$$

$$= -\frac{\mathrm{d}}{\mathrm{d}t}\frac{\mu_0}{4\pi}\int_C \frac{\boldsymbol{m}\times\boldsymbol{r}'}{r^3}\cdot\mathrm{d}\boldsymbol{l} = +\frac{\mathrm{d}}{\mathrm{d}t}\underbrace{\frac{\mu_0}{4\pi}\int_C \frac{\boldsymbol{r}\times\mathrm{d}\boldsymbol{l}}{r^3}}_{=-\boldsymbol{B}_1/I}\cdot\boldsymbol{m} \tag{1.41}$$

$$= -\frac{\mathrm{d}}{\mathrm{d}t}\frac{1}{I}\boldsymbol{B}\cdot\boldsymbol{m} \tag{1.42}$$

Note the relation $\boldsymbol{r}' = -\boldsymbol{r}$, since in the case of the Biot-Savart law we are looking away from the coil to the point of the magnetic moment, whereas in the case of the vector potential we are interested in the vector potential at the distance $\boldsymbol{r}'$ from the magnetic moment.[4]

4: Thanks to Mengjia He for spotting this error!

Now recall that magnetization is defined as magnetic moment per unit volume. Thus, to get the voltage for *all* magnetic moments, we replace the magnetic moment with the magnetization, and integrate over the volume.

$$V = -\frac{\mathrm{d}}{\mathrm{d}t}\frac{1}{I}\iiint \boldsymbol{B}\cdot\boldsymbol{M}\mathrm{d}V \tag{1.43}$$

This is the principle of reciprocity: The voltage induced in the coil by a precessing magnetic moment is the larger, the larger the magnetic field generated by the coil at the place of the precessing magnetic moment.

If the magnetization and the magnetic field are constant across the sample volume, and if the magnetization precesses in the transverse plane according to $M_x = M_0\sin(\omega t)$, this simplifies to

$$V = -\frac{B_1}{I}\omega M_0 V_s\cos(\omega t) \tag{1.44}$$

Since a good detector will have a homogeneous B_1 accross the sample, it can be seen that the signal scales exactly as *magnetic field per current*.

1.4.2 The duration of a $\pi/2$ pulse*

It is frequently useful to estimate the strength of the B_1 field for a given circuit. Such an estimate has been given by Slichter [6].

[6]: Slichter (1990), 'Principles of Magnetic Resonance'

An inductor carrying a current I stores an energy

$$\frac{1}{2}LI^2. \tag{1.45}$$

But this energy is really the energy of the field that is produced by the current, so we may write

$$\frac{1}{2}LI^2 = \frac{1}{2}\iiint \boldsymbol{MB}\mathrm{d}V = \frac{1}{2\mu_0}B^2V_c \tag{1.46}$$

where we have assumed that the field is homogenoeus and contained in the coil with volume V_c.

In steady state, the power dissipated in the coil equals the power provided by the RF amplifier. We therefore have

$$\frac{1}{2}RI^2 = P \quad I^2 = \frac{2P}{R}. \tag{1.47}$$

Substituting this into equation (1.46), we get

$$\frac{1}{2}\frac{L2P}{R} = \frac{1}{2\,\mu_0}B^2V_c. \tag{1.48}$$

Now we use the relation $Q = \omega L/R$, and solve for B:

$$B = \sqrt{\frac{QP2\mu_0}{\omega V_c}}. \tag{1.49}$$

Now the field generated by the coil is linearly polarized, and has to be decomposed into two circularly polarized fields, e.g.

$$B = B_1\exp(\mathrm{i}\omega t) + B_1\exp(-\mathrm{i}\omega t). \tag{1.50}$$

Therefore

$$B_1 = B/2 = \sqrt{\frac{\mu_0 QP}{2\omega V_c}}. \tag{1.51}$$

[7]: Doty et al. (1988), 'Noise in High-Power, High-Frequency Double-Tuned Probes'

In this equation Q is readily measured by the width of the return loss spectrum 7 dB below the baseline [7].

We can now calculate the nutation frequency $\omega_1 = |\gamma B_1|$, and use $\omega_1\tau_{\pi/2} = \pi/2$ to calculate the duration of a $\pi/2$ pulse $\tau_{\pi/2}$.

[8]: Nyquist (1928), 'Thermal Agitation of Electric Charge in Conductors'

1.4.3 The noise

The electrons in the coil wire generate a noise voltage, which is known as Johnson or Nyquist noise [8]. The noise voltage is given by

$$V_N = \sqrt{4kTR\Delta f}. \tag{1.52}$$

[9]: Kovacs et al. (2005), 'Cryogenically Cooled Probes-A Leap in NMR Technology'

Here, Δf is the bandwidth over which the noise is measured, T is the coil's temperature, and R is its resistance. It can be seen that cooling the coil is a very good idea - it lowers the temperature T *and* the resistance R. Indeed, cryoprobes can give an approximately 4-fold increase in SNR.[9]

1.5 The Signal-to-Noise Ratio of the NMR Experiment

The Signal-to-Noise Ratio (SNR) of the NMR experiment is simply the ratio of the signal and the noise voltages. In practice, the SNR is lower, because the preamplifier adds a bit of *extra* noise to the signal. It is possible to increase the SNR by averaging more than one acquisitions. The NMR signal is the same in every acquisition, but the noise is different. When averaging, the SNR increases with the square-root of the number of acquisitons, or equivalently, with the square root of time.

It should be stressed that there are many ways to increase the SNR that do *not* rely on hyperpolarization. These range from adding paramagnetic impurities to increase the cycle time, to pulse sequences such as INEPT that report on insensitive low-γ nuclei by exploiting their couplings to sensitive high-γ nuclei, to parallel acquisition. For a review of these techniques, see [10].

[10]: Kupče et al. (2021), 'Parallel Nuclear Magnetic Resonance Spectroscopy'

1.6 Concluding Remarks

In this lecture we have seen that the NMR signal is proportional to the nuclear spin polarization, and that the latter is very small. By contrast, the electron spin has a much larger polarization, and becomes almost fully polarized at low temperatures. We have already mentioned briefly that the large electron polarization can be transferred to nuclear spins. This transfer is known as dynamic nuclear polarization. A sample is hyperpolarized in this way will relax to thermaal equilibrium as soon as the DNP process is stopped. At the same time, relaxation can give us valuable insight into molecular structure and dynamics. Relaxation is therefore the topic of the next lecture.

1.7 Further Reading*

Here I give a few additional references which have not been cited in the lecture.

- This lecture can be no substitute for a thorough introduction to central concepts of magnetic resonance, including angular momentum, spin operators and the density matrix. An excellent, detailed introduction to these topics has been given by Levitt [11].
- To read about the art of discerning signal and noise in disciplines outside NMR, such as meteorology, climate change, or financial markets, have a look at Silver's excellent book "The Signal and the Noise: The Art and Science of Prediction" [12].

1.8 Python*

In this lecture we will be using Python for everything from evaluating simple expressions to setting up Hamiltonians and systems of differential equations.

You can use any other tool that does the job for you, but the tool should allow you to carry out matrix multiplication in a simple way.

If you choose to give Python a go, the Anaconda Python distribution[5] is a good start. On Linux systems you already have Python. On Windows, if you don't want to install anything, you can use WinPython [6]. Both Anaconda and WinPython come wiht a server for Jupyter notebooks and Jupyter lab.

5: Available from https://www.anaconda.com/products/distribution

6: Available from http://winpython.github.io/

Once you have python up and running, you can run

```
pip install spindata
```

The spindata module stores the gyromagnetic ratios of all NMR active nuclei, and the electron. An example is shown below. The code below loads the numpy module (which stores π as np.pi), and the spindata module. The last line is a print statement that prints the given number dE / (2*np.pi*1e6) as a float with two digits after the decimal point. The code is best run inside a Jupyter Notebook.

```
# import numpy module
import numpy as np

# import spindata module
from spindata import gamma

# magnetic field in Tesla
B = 1

# calculate energy splitting
dE = gamma("1H")*B

print("{:.2f} MHz".format(dE / (2*np.pi*1e6))
```

For the electron use "E" instead of "1H".

Constants such as $\hbar$ and the Boltzmann constant k are made available in Python by running

```
from scipy.constants import hbar, k
```

1.9 Exercises

1. Give the matrix representation of $\hat{I}_z$ in the Zeeman basis for a spin $I = 3/2$. Do this first on paper, then create it in Python using the np.diag command, and finally create the matrix representation for an arbitrary half-integer or integer spin using a for loop.
2. Calculate the polarization of (i) free electron spins at 6.7 Tesla and 1 Kelvin, and (ii) ^{13}C at the same field, but at 300 Kelvin. What is the ratio of the two?

3. A hyperpolarization method supplies a bolus of liquid containing a molecule of interest with a polarization that is 10,000 times higher than the thermal equilibrium polarization in the magnet. However, the hyperpolarization method leads to a 20-fold dilution of the analyte. The hyperpolarization experiment can be run every hour, but the analyte has a short T_1 of 0.2 s, and the acquisition on the thermal equilibrium sample can be run every second. How do the SNRs of hyperpolarization and "brute-force" compare after 1 hour? You find out that no one is using the spectrometer, and run the experiment for another 15 hours. How do the SNRs compare now?
4. The proton channel of your new 400 MHz probe has a Q of 200, and a coil volume of 0.5 mL. Calculate the B_1 and the duration of a $\pi/2$ pulse for an RF power of 50 W.

Relaxation 2

2.1 The Main Ideas

Relaxation is a systems transition to equilibrium after a perturbation. Examples for such a perturbation in magnetic resonance are

- A π pulse inverts populations. After the inversion the populations approach their thermal equilibrium value with a time constant T_1.
- A $\pi/2$ pulse equilibrates populations and creates coherences (off-diagonal entries in the density matrix). The coherences vanish in thermal equilibrium, and decay with a time constant T_2. The populations again approach thermal equilibrium with a time constant T_1.
- Changes of magnetic field and temperature change the thermal equlibrium polarization. The system again approach the new thermal equilibrium value with a time constant T_1.

In many cases, the spin relaxation cannot be described by a single time constant. However, these cases are outside the scope of this introductory lecture.

We can think of T_1 as a friction process that enables the return of the spins to their resting position. This is analogous to a swing that has been pulled away from its resting position. During a period of the swing potential and kinetic energy are converted. However, over time, friction in the bearings of the swing and friction with the air convert this energy to heat, and the swing amplitude decreases until, eventually, it reaches zero.

In nuclear magnetic resonance, relaxation is not caused by mechanical friction, but by *fluctuating fields*.

We will discuss different mechanisms that give rise to fluctuating fields, and see how the time dependence of the fluctuating fields leads to frequency-dependent spectral densities.

2.2 Relaxation Mechanisms

- `Dipole-dipole Relaxation`. The dipole-dipole interactionb between two nuclei is an *anisotropic* interaction, i.e. it depends on the angle between the vector connecting the two nuclear spins and the vector indicaating the direction of the applied magnetic field B_0. Correspondingly, as the molecule tumbles, the spin interactions within the molecule (intramolecular interactions), as well as the spin interactions across molecules (intermolecular interactions) change in time, causing relaxation. Dipolar interactions also exist between electron spins (e.g. of stable radicals) and nuclear spins. Due to the large gyromagnetic ratio of the electron spin, electron-nuclear spin interactions can be very strong. We can think of dipolar interactions as one spin producing a time-dependent magnetic field at the site of the other spin.

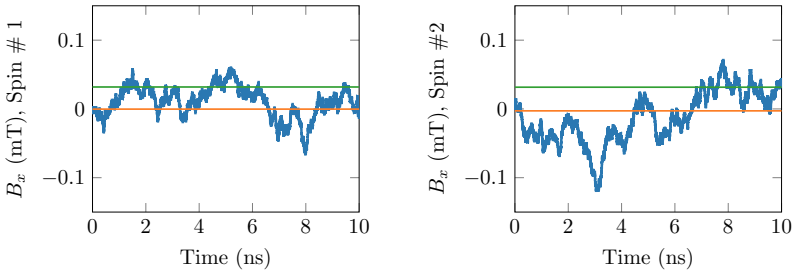

Figure 2.1: Simulated random fields as experienced by two spins labelled #1 and #2. The fields experienced by the two spins are uncorrelated. They have zero mean value $\langle B_X \rangle = 0$, but a non-zero root mean square, $\sqrt{\langle B_X^2 \rangle} > 0$. Note that the fields are not completely randomn. For example knowledge of the value of B_X at a certain point in time enables a decent prediction of the field 0.1 ns later. Such a relatively long "memory time" is characeteristic of a large molecule in solution that, due to its slow motion, experienceses more slowly varying fields. Note that a relatively long simulation is required to get stable values for the averaged quantities. The simulations above have been run for 500 ns, but only the first 10 ns of the simulation are shown.

- `Chemmical Shift Anisotropy (CSA)`. The shielding of the applied magnetic field, known as chemical shift is also *anisotropic.*[1] In liquids, the fast motion aaverages the chemical shift to an isotropic value. Since the shielding depends on the orientation of the molecule with respect to the applied field, it will change in time. This can again be expressed as a time-dependent magnetic field experienced by the spin. The CSA mechanism increases in importance as the magnetic field is increased. It is also more important for nuclei with a large chemicala shift range, such as ^{19}F.
- `Spin Rotation`. This mechanism is effective for rapidly rotating small molecules, in particular in the gas phase.
- `Quadrupolar Relaxation`. This mechanism can be very effective, but is active only for spins with a quadrupolar nucleus, i.e. with a spin $I > 1/2$.

1: A single value is given for molecules in solution. This is because the rapid molecular motion leads to an averaging of the chemical shift over all possible values. In solids, where this motion is absent, the chemical shift anisotropy is readily obbserved as a characteristic roadening of the spectral resonance.

All of these relaxation mechanisms in essence create random fields that fluctuate in time. Typical time dependences are shown for two different spins in Fig. 2.1.

2.3 The Autocorrelation Function

It is plausible that the randomn fields cause relaxation if they fluctuate at or near the nuclear Larmor frequency. Then we can think of them as a continuous train of RF pulses with random amplitude and phase that will ultimately disperse any non-equilibrium magnetization.

The speed of the flucutations is measured by the autocorrelation function. The autocorrelation simply measures how much $B_X(t)$ changes, if we shift it by a time τ:

$$G(\tau) = \langle B_X(t) B_X(t+\tau) \rangle \tag{2.1}$$

Clearly, $G(0) = \left\langle B_X(t)^2 \right\rangle > 0$, since this is an average over the square of $B_X(t)$, which is always positive. However, as we increase τ to large values, there will be no correlation between $B_X(t)$ and $B_X(t+\tau)$, so that their product will sometimes be positive, sometimes negative, and average to zero.

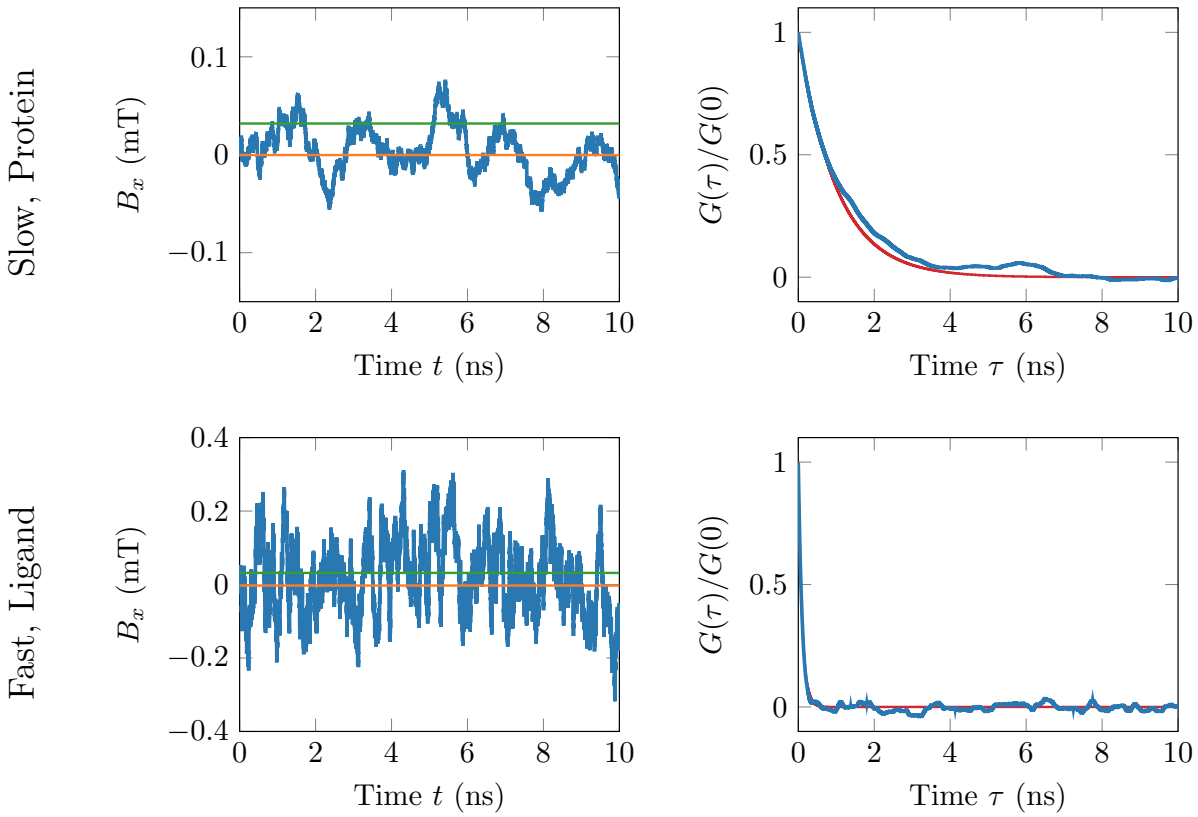

Figure 2.2: Slowly changing random fields (top) as they are encountered by a slowly tumbling protein, and more rapidly changing fields (bottom) as they are encountered by a small molecue such as a ligand or fragment. The plots on the left show the fluctuating field in time. Note that the more rapidly fluctuating field has the same root mean square value as the slowly evolving field. The numerical values for the correlation function are shown as blue lines on the right, together with an exponential fit with a decay constant of 1 ns (slow, top) and 0.1 ns (fast, bottom). Note that again the simulation has been run for 500 ns in both cases, and only the first 10 ns are shown.

The time dependence of the random fields in Fig. 2.1 has been calculated by starting with a value of 0 at $t = 0$. Then 1 ps (picosecond) later the new field is calulated as 0.999 times the oldfield + 0.001 times a random number between $-1/2$ and $+1/2$, i.e. the field is allowed to change by 1 permill in a randomn direction every ps. This procedure gives rise to an exponentially decaying correlation function with a correlation time constant τ_C =1 ns, as shown in the top right panel in Fig. 2.2.

For a small molecule, the reorientation happens faster, and so the random field may also change more quickly in time. Starting again with a value of 0 at $t = 0$, the new field is calculated as 0.99 times the old field + 0.01 times a random number between $-1//2$ and $+1/2$. This procedure gives rise to a tiime dependence of the fluctuating field asa shown in the left bottom panel of Fig. 2.2. Its autocorrelation function (shown in the bottom right panel), is well described by an exponential decay with a time constant $\tau_c = 0.1$ ns.

In many cases, it is appropriate to assume an exponential decay of $G(\tau)$, i.e.:

$$G(\tau) = \left\langle B_X^2(t) \right\rangle \exp\left(-\tau/\tau_c\right) = G(0) \exp\left(-\tau/\tau_c\right) \tag{2.2}$$

The time constant τ_c is referred to as correlation time.

As the temperature is increased, τ_C becomes shorter, due to more rapid motion in the sample. As the temperature is reduced, τ_c becomes longer.

Large molecules have a longer correlation time than small molecules, since they change orientation more slowly.

2.4 Spectral Density

As we have mentioned earlier, In order to drive relaxation, we need fields that fluctuate at or near the Larmor frequency. But what is the frequency spectrum of the fluctuating random fields? We obtain this spectrum by calculating the Fourier transformm of the spectral density:

$$\tilde{\mathcal{J}}(\omega) = \int_0^\infty G(\tau)\exp(-\mathrm{i}\omega\tau)\mathrm{d}\tau \tag{2.3}$$

Since we assume $G(\tau)$ to decay exponentially with time constant τ_c, we have to calculate the Fourier Transform of an exponential decay. The result is a Lorentzian:

$$\tilde{\mathcal{J}}(\omega) = 2G(0)\frac{\tau_C}{1+\omega^2\tau_C^2} \tag{2.4}$$

2: This is not a trivial exercise. However, one can think of the random fields as "miniature random radio-frequency pulses". If they oscillate at the Larmor frequency they can induce transitions in the same way that a train of radio freqnuency pulses leads to saturation.

Now, one can use perturbataion theory [13] to calculate the *rates* of transitions between the stataes $|\alpha\rangle$ and $|\beta\rangle$ as indicated in Fig. **??**?[2] The result is

$$W_- = W_+ = \frac{1}{4}\gamma^2\tilde{\mathcal{J}}(\omega) = \frac{1}{2}G(0)\frac{\tau_C}{1+\omega^2\tau_C^2} \tag{2.5}$$

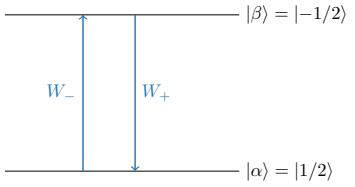

Figure 2.3: The transition from $|\alpha\rangle$ to $|\beta\rangle$ and from $|\beta\rangle$ to $|\alpha\rangle$ occur at rates W_- and W_+ respectively. Since in thermal equilibrium $N_{|\alpha\rangle} > N_{|\beta\rangle}$, W_+ and W_- are not exactly equal, $W_+ > W_-$.

This result however must be *wrong*. If the rates W_- and W_+ are equal, they will also equalize the populations of the levels $|\alpha\rangle$ and $|\beta\rangle$, and there would be no polarization. Our theory gives the wrong result, because the random fields produced by the molecular rotation will *not* be entirely random, but will have an ever so slight preference to drive spins to the lower energy $|\alpha\rangle$ state.

We know that eventually there will be thermal equilibrium across the involved transitions, so that the ratio of the populations of the stataes $|\alpha\rangle$ and $|\beta\rangle$ is given by the Boltzmann distribbution:

$$\frac{N_{|\alpha\rangle}}{N_{|\beta\rangle}} = \exp\left(-\frac{\Delta E}{kT}\right) \approx 1 - \frac{\Delta E}{kT}. \tag{2.6}$$

In order to ensure this outcome, one adjusts the rates such that

$$\frac{W_+}{W_-} = \frac{N_{|\alpha\rangle}}{N_{|\beta\rangle}}. \tag{2.7}$$

The spin-lattice relaxation rate is then

$$T_1^{-1} = 2W = \gamma^2 G(0)\frac{\tau_c}{1+\omega^2\tau_c^2} \tag{2.8}$$

Let us look at the extremme cases $\tau_c \to \infty$ and $\tau_c \to 0$.

- If $\tau_c \rightarrow \infty$, the molecule requires infinite time to reorient itself. We then have $\frac{\tau_c}{1+\omega^2\tau_c^2} \approx \frac{1}{\omega^2\tau_c} \rightarrow 0$, i.e. there is very weak to no relaxation. This is the case in solids at very low temperature, i.e. in the abscence of motion.
- If $\tau_c \rightarrow 0$, i.e. the molecule rotates infinitely fast, then $\frac{\tau_c}{1+\omega^2\tau_c^2} \rightarrow 0$, and again there is no relaxation.

Thankfully, molecules exhibit correlation times that are such that efficient relaxation occurs, which is a prerequisite for the buildup of the thermmaal equilibrium signal. The relaxation rate depends on the nucleus, since it scales with the gyromagnetic ratio γ. It depends on the applied magnetic field, since it scales with the Larmor frequency ω. And it depends on the molecule size and the sample temperature, since it depends on τ_c.

2.5 Further Reading*

- For a somewhat more detailed introduction to relaxation have a look at Levitt's spin dynamics [11].
- For a thorough discussion of relaxation, consider the book by Kowalewski and Mäler kowalewski-2006-nuclear-spin.

2.6 Python*

The code below shows you how to generate a random field and calculate its autocorrelation using Python.

```
import numpy as np
import matplotlib.pyplot as plt

def autocorr(x):
    result = np.correlate(x, x, mode='full')
    print(result.size)
    result = result / np.max(result)
    return result[int(result.size/2):]
    #return result


# fast fluctuations, 100 ps

bVals = [0.0]
numberOfPoints = 500001
for t in range(numberOfPoints-1):
    bVals.append(0.99*(bVals[t]) + 0.01*(np.random.rand() - 0.5))


bVals = np.array(bVals)/200 * 1000
plt.plot(bVals)
plt.plot(np.ones(len(bVals))*np.mean(bVals))
plt.plot(np.ones(len(bVals))*np.sqrt(np.mean(np.array(bVals)*np.
    array(bVals))))

yCorrel = autocorr(bVals)
plt.xlim(0, 10000)
```

```
#print(yCorrel)

plt.figure(figsize=(10,5))
plt.plot(yCorrel)

expDecay  = np.exp(-np.arange(numberOfPoints)/100)
plt.plot(expDecay)

plt.xlim(0, 10000)
```

Hyperpolarization 3

3.1 The Main Ideas

The objective of hyperpolarization is to generate a state with a polariyation that is much larger than the thermal equilibrium polarization.

We can write this formally as

$$P \gg P_{th} = \tanh\left(\frac{\hbar\gamma B}{2kT}\right) \approx \frac{\hbar\gamma B}{2kT}. \tag{3.1}$$

Here we have inserted the high-temperature approximation ($\hbar\gamma B \ll kT$).

Note that in thermal equilibrium, and at a fixed field, a high spin polarization corresponds to a low spin temperature T. We can therefore say that we want to cool the spins.

One simple way to achieve hyperpolarization is therefore to cool the sample (and thereby the spins) to a lower temperature. Then, if the temperature is increased rapidly (so that the sample temperature increases rapidly compared to the time scale of nuclear spin-lattice relaxation), the spins will remain at the lower temperature, and only assume the new, lower thermal equilibrium polarization on the T_1 time scale. In practice, this so-called brute-force polarization is not too useful, because very low temperatures (milli-Kelvin) are required to achieve substantial polarization in magnetic fields that are technologically available today (10s of Tesla). At these low temperatures, the spin-lattice relaxation time constant becomes prohibitively long, and the spins never achieve their thermal equilibrium at low temperatures.

A more feasible idea is to instead use electron spins as the source of polarization. Electrons have a 660 times larger gyromagnetic ratio than protons, and attain near-unity polarization at a field of several Tesla and a temperature of 1 Kelvin. The dependence of thermal equilibrium polarization on temperature, for a field of 6.7 Tesla, is shown in Fig. 3.1.

But how can one transfer the large electron spin polarization to nearby nuclei?

- Albert Overhauser was the first to realize in 1952 that in lithium metall this is possible by saturating the electron transition of the conduction electrons using microwave irradiation.
- Shortly after Overhauser, Jeffries and Abragam realized that in insulating solids, such a transfer is possible by driving a simultaneous electron-nuclear transition, a so-called forbidden transition.
- Today, most DNP processes make use of so-called thermal mixing. Here, two electron spins are involved. At low temperatures, both are in their ground-state. Then, microwave irradiation is used to flip one of the spins. After that, a flip-flop (simultaneous change of two electron spin quantum numbers) is possible in which the

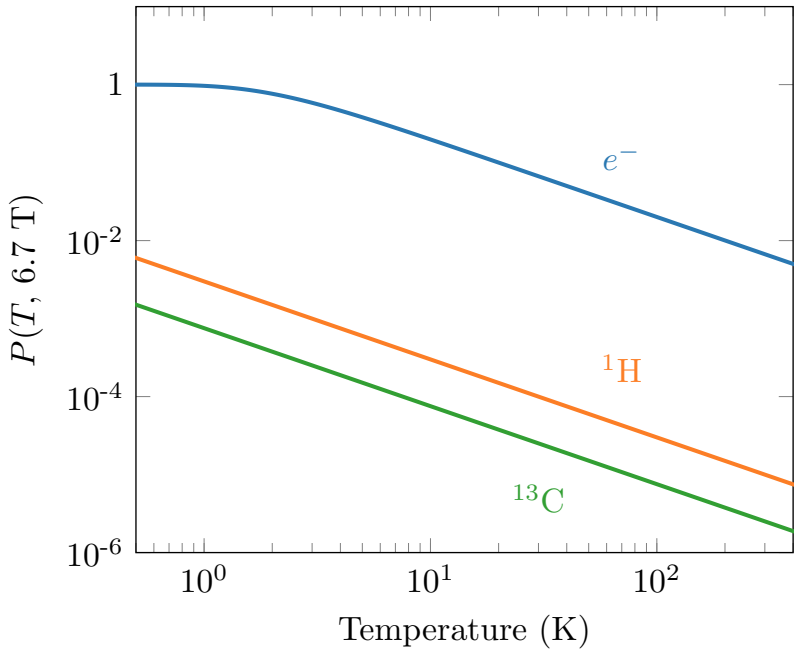

Figure 3.1: Thermal equilibrium polarization for the electron (blue), ^{1}H (orange) and ^{13}C at a field of 6.7 Tesla

energy released or absorbed by the electron spins is absorbed or released by the nuclear spins.

In this chapter we will study the Overhauser effect in greater detail and then briefly review the solid effect and thermal mixing.

3.2 The Overhauser Effect

[1]: Overhauser (1953), 'Polarization of Nuclei in Metals'

[2]: Carver et al. (1953), 'Polarization of Nuclear Spins in Metals'

[3]: Slichter (2010), 'The Discovery and Demonstration of Dynamic Nuclear Polarization-A Personal and Historical Account'

In 1952, then PhD student Albert Overhauser realized that electron polarization in metallic lithium can be transferred to the lithium nuclei by *saturating* the electron spins [1]. This idea was met with some skepticism, but Slichter and Carver validated Overhausers theory experimentally in 1953 [2]. An inspiring account of the "birth of hyperpolarization" has been given by Slichter [3].

The dynamics are described by a set of four differential equations for the four energy levels:

$$\frac{\mathrm{d}p_1}{\mathrm{d}t} = p_2W_{21} - p_1W_{12} + p_4W_{41} - p_1W_{14} + (p_2 - p_1)W_e \tag{3.2}$$

$$\frac{\mathrm{d}p_2}{\mathrm{d}t} = -p_2W_{21} + p_1W_{12} - (p_2 - p_1)W_e \tag{3.3}$$

$$\frac{\mathrm{d}p_3}{\mathrm{d}t} = p_4W_{43} - p_3W_{34} \tag{3.4}$$

$$\frac{\mathrm{d}p_4}{\mathrm{d}t} = p_1W_{14} + p_3W_{34} - p_4W_{43} - p_4W_{41} \tag{3.5}$$

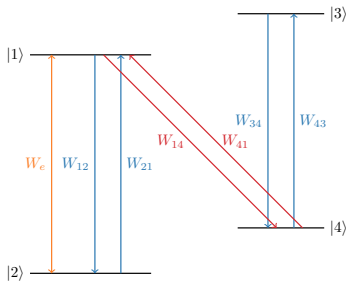

Figure 3.3: The same drawing as 3.4

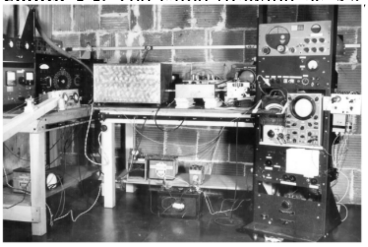

Figure 3.2: The first DNP Spectrometer. Reproduced from Ref. [3]

Once we achieve equilibrium, the transitions do no longer lead to changes in the net population of the respective levels, and

$$\frac{\mathrm{d}p_i}{\mathrm{d}t} = 0. \tag{3.6}$$

The probabilities of being in any particular state have to add to 1:

$$p_1 + p_2 + p_3 + p_4 = 1 \tag{3.7}$$

If W_e is sufficiently strong, we will achieve saturation accross the transition $|1\rangle \leftrightarrow |2\rangle$, and hence

$$p_1 = p_2 \tag{3.8}$$

From Eq. 3.4, we have

$$p_3 = p_4 \frac{W_{43}}{W_{34}}, \tag{3.9}$$

and from Eqs. (3.4) and (3.5) we have

$$p_1 = p_4 \frac{W_{41}}{W_{14}} \tag{3.10}$$

The transition $|3\rangle \leftrightarrow |4\rangle$ is in thermal equilibrium, as is the transition $|1\rangle \leftrightarrow |4\rangle$. The population ratio accross these transitions is hence given by the Boltzmann distribution

$$\frac{p_i}{p_j} = \exp\left(-\left(E_i - E_j\right)/kT\right) \tag{3.11}$$

This may be rewritten as

$$p_i \underbrace{\exp\left(+\left(E_i - E_j\right)/kT\right)}_{B_{ij}} = p_j \tag{3.12}$$

where we have introduced the symbol B_{ij} with

$$p_i B_{ij} = p_j \tag{3.13}$$

and with

$$B_{ij} = 1/B_{ji} \tag{3.14}$$

and

$$\frac{B_{ix}}{B_{kx}} = B_{ik} \tag{3.15}$$

We rewrite Equations (3.9) and (3.10) as

$$p_3 B_{34} = p_4 \tag{3.16}$$

and

$$p_1 B_{14} = p_4 \tag{3.17}$$

Now we use these two expressions to eliminate p_4, and we eliminate p_2 by inserting $p_1 = p_2$ into Eq. (3.7), and we have

$$p_3 B_{34} = p_1 B_{14} \tag{3.18}$$

$$2p_1 + p_3 + p_3 B_{34} = 1 \tag{3.19}$$

We use the first equation to eliminate p_3 in the second, and obtain

$$2p_1 + p_1 \frac{B_{14}}{B_{34}} + p_1 B_{14} = 1 \tag{3.20}$$

and hence

$$p_1 = p_2 = \frac{1}{2 + \frac{B_{14}}{B_{34}} + B_{14}} = \frac{1}{2 + B_{13} + B_{14}} \tag{3.21}$$

We furthermore have

$$p_4 = p_1 B_{14} = \frac{B_{14}}{2 + B_{13} + B_{14}} \tag{3.22}$$

and

$$p_3 = p_4 / B_{34} = \frac{B_{13}}{2 + B_{13} + B_{14}} \tag{3.23}$$

Now let us see whether these populations give rise to stronger NMR signals. To do so, we need to calculate the *nuclear* spin polarization P_n. The nuclear transitions are the ones involving the states $|1\rangle$ and $|3\rangle$ on the one hand, and $|2\rangle$ and $|4\rangle$ on the other. The nuclear spin polarization is the sum of the polarization of the two relevant transitions:

$$P_n = (p_1 - p_3 + p_2 - p_4) \tag{3.24}$$

$$= \frac{2 - B_{13} - B_{14}}{2 + B_{13} + B_{14}} \tag{3.25}$$

Note that the transition stil ranges between -1 and $+1$, because $\sum p_i = 1$.

Now we insert the high-temperature approximation $B_{ij} \approx 1 + \frac{(E_i - E_j)}{kT}$, etc. Then we have

$$P_n = \frac{2 - \left(1 + \frac{E_1 - E_3}{kT}\right) - \left(1 + \frac{E_1 - E_4}{kT}\right)}{4} \tag{3.26}$$

$$= -\frac{(E_1 - E_3) + (E_1 - E_4)}{4kT} \tag{3.27}$$

$$= -\frac{2E_1 - E_3 - E_4}{4kT} \tag{3.28}$$

The dominant electron Zeeman energy is $E_1 \sim \frac{1}{2}\gamma_e B$ in level, where as the same terms $-\frac{1}{2}\gamma_e B$ cancel each other in levels 3 and 4. As usual, $\gamma_e = \mu_B g/\hbar$ is the gyromagnetic ratio of the free electron spin with g-factor $g \approx 2$ for radicals as they are typically used in DNP, and μ_B being the Bohr Magneton. Then we have

$$P_n = -\frac{\hbar \gamma_e B}{4kT} \tag{3.29}$$

On the other hand, from the first lecture, we have for nuclear spins at thermal (th) equilibrium

$$P_n^{\text{th}} = \frac{\hbar \gamma_I B}{2kT} \tag{3.30}$$

The ratio of these two is

$$\frac{P_n}{P_n^{\text{th}}} = \frac{\gamma_e}{2\gamma_I} \tag{3.31}$$

If one saturates both transitions, the factor two disappears, and the enhancement is

$$\frac{P_n}{P_n^{\text{th}}} = \frac{\gamma_e}{\gamma_I} \tag{3.32}$$

which corresponds to ≈ 660 for protons, and is even larger for nuclei with a lower gyromagnetic ratio.

3.3 The Solid Effect*

In insulating solids, there is no efficient cross-relaxation mechanism, and microwave irradiation of the electron transition does in general not lead to hyperpolarized NMR transitions.

In 1957, Jeffries [14] and indepentenly Abragam realized that in such cases one may still drive enhance the nuclear spin polarization by driving a "forbidden" transition.[1]

[14]: Jeffries (1957), 'Polarization of Nuclei By Resonance Saturation in Paramagnetic Crystals'

1: The concept of forbidden transitions is beyond the scope of this lecture. In practice, driving a forbidden transition requires strong microwave sources. The transition becomes "more forbidden" as the applied magnetic field is increased, requiring ever stronger microwave sources (up to 100s of Watts, compared to typically 100 mW that are used in typical dissolution DNP experiments).

We can derive the enhancement of the solid effect in a fully analogue way to that of the Overhauser effect. The microwave irradiation saturates the $|1\rangle \leftrightarrow |4\rangle$ transition, so

$$p_1 = p_4. \tag{3.33}$$

On the other hand, there is a thermal equilibrium over the $|1\rangle \leftrightarrow |2\rangle$ and $|3\rangle \leftrightarrow |4\rangle$ transitions, so

$$p_3 B_{34} = p_4 = p_1 \quad ; \quad P_1 B_{12} = p_2. \tag{3.34}$$

From $p_1 + p_2 + p_3 + p_4 = 1$, we have

$$2p_1 + p_1 B_{12} + p_1 B_{43} = p_1(2 + B_{12} + B_{43}) = 1 \Rightarrow p_1 = \frac{1}{2 + B_{12} + B_{43}} \tag{3.35}$$

The polarisation is again the difference accross the NMR transitions, which, using $p_1 = p_4$ is

$$P = p_2 + p_1 - p_4 - p_3 = p_2 - p_3 = p_1 (B_{12} - B_{43}) \tag{3.36}$$

$$= \frac{B_{12} - B_{43}}{2 + B_{12} + B_{43}} \approx \frac{B_{12} - B_{43}}{4} \approx \frac{2\hbar\gamma_e B}{4kT} \tag{3.37}$$

When comparing this with our standard expression for the nuclear expression in the high-temperature approximation (3.30), we see that the enhancement is again γ_e/γ_I.

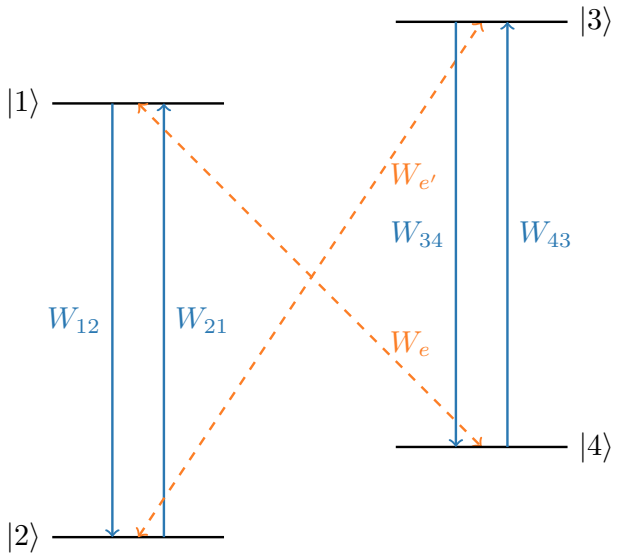

Figure 3.4: The same diagram as 3.3. In the solid effect, a relaxation mechanism for transitions such as $|1\rangle \leftrightarrow |4\rangle$ is absent. However, the transition may be driven by microwave irradiation. Depending on the frequency of the microwave irradiation either positive W_e or negative nuclear spin polarizatoin W_e' is obtained.

3.4 Thermal Mixing*

The third member of the family of DNP mechanisms is thermal mixing. In contrast to the Overhauser and Solid Effect, Thermal Mixing requires two electron spins. The process is shown schematically in Fig. 3.5.

In thermal mixing, first all electron spins are polarized by keeping them in a high magnetic field. Each pair of electron spins is then in the state $|--\rangle$. The spins have a slightly different environment, such that we can flip them selectively. Suppose that we apply microwave irradiation to selectively flip the first electron spin, such that the state becomes $|+-\rangle$. Now a flip flop can occur, in which the electrons swap their quantum numbers, i.e. the electron spin state becomes $|-+\rangle$. However, because the electron spins have a slightly different environment, this flip flop will change the energy of the spin pair. That change in energy is balanced by a change in the nuclear spin energy. For example, if the state $|-+\rangle$ is higher in energy than $|+-\rangle$, the flip flops will absorbb energy from the nuclear spins. We can think of this as cooling the nuclear spins, hence the term thermal mixing.

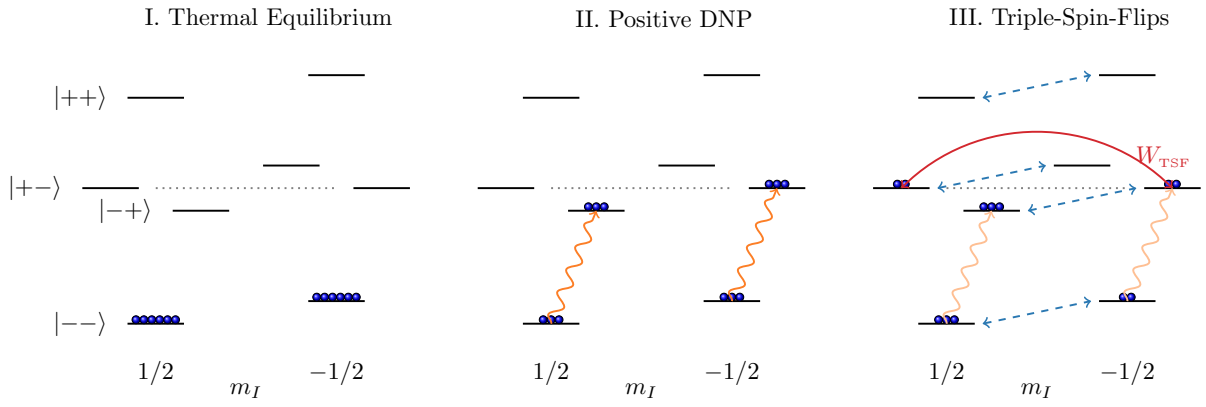

Figure 3.5: Triple-Spin-Flips. (I) In thermal equilbrium the electron spin ground state is more strongly populated than the excited states. Note that each state is characterized by two qunatum numbers for the two electron spins (such as $|+-\rangle$), and the nuclear quantum number m_I (with values $1/2$ and $-1/2$). The product states are written as $|+-\rangle \otimes |m_i\rangle = |+-m_I\rangle$. Note furthermore, that the energy difference an electron-electron flip-flop, i.e. $|+-\rangle \leftrightarrow |-+\rangle$ corresponds exactly to the energy difference of a nuclear spin flip, as indicated by the dotted line. This is the matching condition for triple-spin-flips. The energy difference between the two electron configurations can be brought about by electron Zeeman anisotropy (which is the dominant contribution in the cross-effect) and/or by spin-spin interactions. (II) The two degenerate electron transitions $\left|--\frac{1}{2}\right\rangle \leftrightarrow \left|-+\frac{1}{2}\right\rangle$ and $\left|---\frac{1}{2}\right\rangle \leftrightarrow \left|-+-\frac{1}{2}\right\rangle$ are saturated using microwave irradiation. (III) The triple-spin-flip $\left|-+-\frac{1}{2}\right\rangle \leftrightarrow \left|+-\frac{1}{2}\right\rangle$ equilibrates the populations of the participating, degenerate levels. The result is a strong positive polarization accross the nuclear spin transitions (dashed blue arrows). By the same processes, applying microwave irradiation at a higher frequency (i.e. across the $|--\rangle \leftrightarrow |+-\rangle$ transition) would lead to negative polarization (not shown).

Ligand Binding 4

4.1 The Main Ideas

Ligand binding describes the typically reversible binding of small molecules to larger molecules. In a typical setting, the large molecules are proteins that are associated with a certain disease. A drug works by binding to to the protein, and therefore our task is to identify those molecules that bind to the protein, and to determine the binding strength.

NMR currently has a much lower throughput then other methods that are in use for identifying drug candidates. However, NMR is unique in that it can probe binding under physiological conditions, and probe both ligand and protein integrity as the binding is observed. Consequentially, NMR does not suffer from false positives. In a typical pharmaceutical setting, a high-throughput assay is used to find drug candidates, and then NMR is used to validate the findings. For a detailed description of NMR in drug discovery we refer to the excellent review by Alvar Gossert and Wolfgang Jahnke [15].

The promise of combining hyperpolarization and ligand-binding is that this combination may dramatically increase the throughput of NMR based drug screening. However, we will see that hyperpolarization has other benefits to offer. For example, hyperpolarization may be used to dramatically reduce the required amount of protein, or it may be used to extend the scope of NMR studies to ligands which bind strongly to their targets.

We will first introduce the concept of ligand binding, and then look in detail at two classical experiments for assessing ligand binding, namely the saturation transfer difference experiment and the so-called waterLOGSY experiment.[1].

1: I thank Pooja Narwal and Pooja Singh for recording the NMR data that is presented as part of this lecture

4.2 Ligand binding concepts

A sketch of a small molecule (the ligand L) binding to a large molecule (the protein P) is shown in Fig. XX. A fragment is a small ligand that may likewise bind to the protein with a small affinitiy (due to its smaller surface area). In Fragment-Based Screening (FBS), one seeks to first identify fragments that bind to a given target. Then these fragments can be combined into a larger ligand that (due to its larger surface area), may exhibit a larger affinity to the protein.

We denote the concentrations of the ligand with $[L]$, those of the protein with $[P]$, and those of the protein-ligand complex with $[LP]$.

In thermal equilibrium, the ratio of free ligand $[L]$ and protein $[P]$ on the one hand, and protein-ligand complex $[LP]$ on the other is constant and called the dissociation constant K_D:

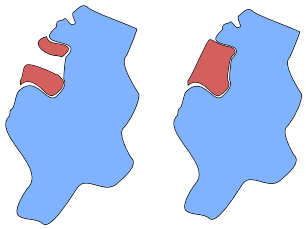

Figure 4.1: Fragment- and Ligand-Binding to a protein. On the left, two fragments (red) are bound to the protein (blue). The picture on the right shows the binding of a (larger) ligand to the same protein.

$$K_D = \frac{[P][L]}{[LP]} \tag{4.1}$$

This ratio also equals the ratio of the rates with which the ligand dissociates and associates with the protein:

$$K_D = \frac{k_{\text{off}}}{k_{\text{on}}} \tag{4.2}$$

For strong binders, the concentration of $[LP]$ is high, and hence the value of K_D is low, with typical values being of the order of 10^{-15} Mol.

Drugs have typical dissocation constant near the nM range, i.e. from 10^{-10} M to 10^{-8} M.

Small fragments bind even less strong, with values in the range from 10^{-5} M to 10^{-3} M.

4.3 The fraction of bound ligand - ligand excess

From our treatment of relaxation, we have seen that small and large molecules have different relaxation times. The ligand's relaxation will therefore depend on whether it is bound to the protein (making it a large molecule) or not. Since the exchange is typically fast compared to the NMR time scale, the measured relaxation rate $R_{1,\text{meas}}$ will be the *weighted average* of the relaxation rates of the free and bound ligand:

$$R_{1,\text{meas}} = \frac{[L_1]R_{1,\text{free}} + [LP]R_{1,\text{bound}}}{[L] + [P]} \tag{4.3}$$

In conventional NMR experiments, there are limits to the protein solubility which imply that the ligand cannot be detected at concentrations of the protein, and one works with ligand excess, $[L] \gg [P]$. However, this implies that the average will be dominated by $R_{1,\text{free}}$, and a simple measurement of the relaxation rate will not reveal whether the ligand binds or not. We will later see two clever ways in which ligand-binding can still be detected in this regime. Of coourse, if we can hyperpolarize the ligand, we may be able to work with a ligand concentration close to the protein concentration, so that the average value $R_{1,\text{free}}$ does report on binding again..

In the experiment, we know how much ligand $[L]_{\text{tot}}$ and protein $[P]_{\text{tot}}$ we add, but we do not know a priori how much free and bound ligand and protein we will have. However, we know that all ligand is either free or bound, and all protein is also free or bound:

$$[L]_{\text{tot}} = [L] + [LP] \tag{4.4}$$

$$[P]_{\text{tot}} = [P] + [LP] \tag{4.5}$$

Together with Eq. (4.1) we have three equations for the three unknowns $[L]$, $[P]$, and $[LP]$. Note that we assume that K_D is known because we want to obtain an expression for $[LP]$ that depends on K_D, so that we can later fit our data to determine K_D.

We now assume that we have substantially more ligand than protein in the solution, so that we can approximate $[L]_{\text{tot}} \approx [L]$.

Solving Eq. (4.1) for $[P]$, we get

$$[P] = \frac{K_D[PL]}{[L]} \tag{4.6}$$

Insertion of this expression into the sum formula for the protein, (4.5) yields

$$[P]_{\text{tot}} = \frac{K_D[PL]}{[L]} + [PL] = [PL]\left(1 + \frac{K_D}{[L]}\right), \tag{4.7}$$

and therefore

$$[PL] = \frac{[P]_{\text{tot}}}{1 + K_D/[L]} = \frac{[P]_{\text{tot}}[L]}{[L] + K_D} \tag{4.8}$$

Since we have an excess ligand concentration, $[L]_{\text{tot}} \approx [L]$, it follows that

$$[PL] = \frac{[P]_{\text{tot}}[L]_{\text{tot}}}{[L]_{\text{tot}} + K_D} \tag{4.9}$$

4.4 The fraction of bound ligand - general case*

In particular in hyperpolarization experiments, we may want to work with ligand concentrations that are close to the protein concentrations. Then, we cannot use the above approximation, but instead we have to insert Eq. (4.8) into Eq. (4.5) and solve the resulting quadratic equation for $[P]$.

The result is given here without derivation:

$$[P] = -\frac{K_D + [L]_{\text{tot}} - [P]_{\text{tot}}}{2} + \sqrt{\frac{(K_D + [L]_{\text{tot}} - [P]_{\text{tot}})^2}{4} + [P]_{\text{tot}}K_D} \tag{4.10}$$

and, by symmetry

$$[L] = -\frac{K_D + [P]_{\text{tot}} - [L]_{\text{tot}}}{2} + \sqrt{\frac{(K_D + [P]_{\text{tot}} - [L]_{\text{tot}})^2}{4} + [L]_{\text{tot}}K_D} \tag{4.11}$$

We also have

$$[PL] = [P]_{\text{tot}} - [P] \tag{4.12}$$

$$= +\frac{K_D + [L]_{\text{tot}} + [P]_{\text{tot}}}{2} - \sqrt{\frac{(K_D + [L]_{\text{tot}} - [P]_{\text{tot}})^2}{4} + [P]_{\text{tot}}K_D} \tag{4.13}$$

$$= \frac{K_D + [L]_{\text{tot}} + [P]_{\text{tot}} - \sqrt{(K_D + [L]_{\text{tot}} - [P]_{\text{tot}})^2 + 4[P]_{\text{tot}}K_D}}{2} \tag{4.14}$$

$$= \frac{K_D + [L]_{\text{tot}} + [P]_{\text{tot}} - \sqrt{(K_D + [L]_{\text{tot}} + [P]_{\text{tot}})^2 - 4[P]_{\text{tot}}[L]_{\text{tot}}}}{2} \tag{4.15}$$

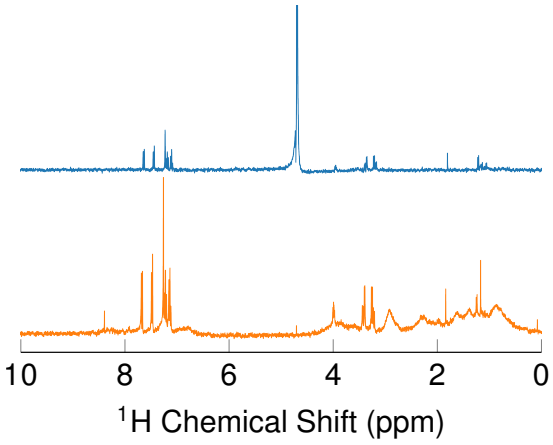

Figure 4.2: Spectra of Tryptophan (top, blue), and a Tryptophan / BSA mixture (bottom, orange) in buffer solution. The tryptophan signals appear between 8 and 8 ppm, and between 3 and 4 ppm. The strong signal at4.7 ppm in the top spectrum is the (unsuppressed) water resonance. The signals between 2 and 1 ppm are attributed to the buffer. The addition of the protein (bottom spectrum) adds broad, unresolved resonances between 0 and 4 ppm.

4.5 Setting the Scence - The Tryptophan / BSA System

We will now focus on one specific system, namely the amino acid *tryptophan* and the protein *bovine serum albumin* (BSA). We first need to get an idea of the NMR spectra of these two compounds. Spectra of tryptoan in buffer solution, and tryptophan+BSA in buffer solution are shown in Fig. **??**. The tryptophan signals are readily identified by comparison with an online database such as the Biological Magnetic Resonance Data Bank (BMRB). Importantly, the aromatic tryptophan signals appear between 7 and 8 ppm.

Addition of BSA to the sample leads to the appearance of broad resonances between 0 and 4 ppm.

4.6 The Saturation-Transfer-Difference Experiment

The key idea of the saturation-transfer-difference (STD) Experiment is that saturating the protein will also lead to saturation of the ligand if the ligand binds reversibly to the protein.

To see this, suppose that a ligand first binds to a protein, and then the saturation pulse is applied to the protein (i.e. to the feature between 0 and 4 ppm). Then, due to spin diffusion, all the protons on the ligand that is bound to the protein will get saturated. Then, if the protein releases the ligand, also the free ligand signals (easily observable between 7 and 8 ppm) will decrease. In practice, the saturation pulse is applied for a long time (several milliseconds), and during this time many ligands bind to the protein, become saturated, and are released back into solution. Consequentially, saturation of the protein can bring about a significant reduction in the ligand signal, even if the ligand concentration exceeds the protein concentration by a factor of 100.

The ability to work with large ligand excess is a key advantage of the STD experiment, since the large ligand concentration makes it easy to detect changes in the signal intensity of the latter.

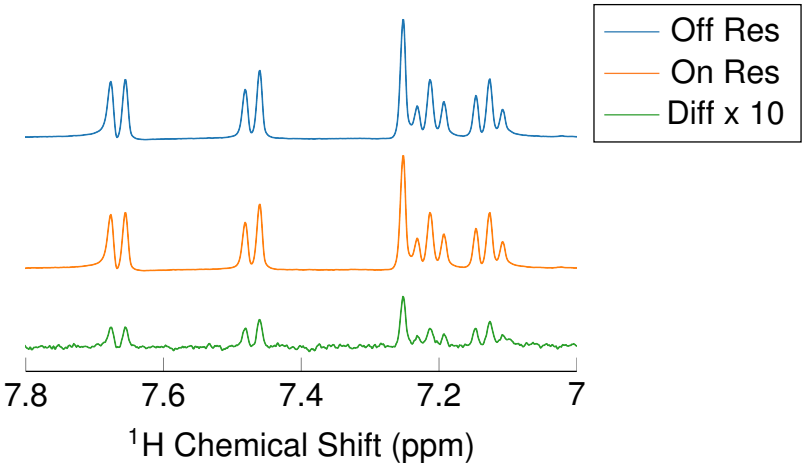

Figure 4.3: Aromatic part of spectra of a Tryptophan / BSA mixture (bottom orange) in buffer solution. In the top blue spectrum, a 1 s saturation pulse is applied at a resonance offset of 40 ppm. With such a huge resonance offset, the pulse cannot saturate the protein, however it may lead to a small signal reduction due to sample heating. For the second, orange spectrum, the 1 s pulse is applied at a resonance offset at 0 ppm, effectively saturating the protein. At first sight, the spectra appear identical, however the difference (green, magnified 10 times) reveals that the orange signal is *weaker* than the blue signal. The difference cannot be due to sample heating since the sample heating will be the same in both experiments. Hence, the difference has to be due to saturation of the ligand that can only occur when the ligand is bound to the protein.

4.7 Determination of K_D based on the STD Experiment*

As long as the saturation pulse is applied, the signal of the free ligand decays. The decay must be proportional to the fraction of ligand that is bound to the protein, which, for excess ligand concentration is Eq. (4.9). Naively, we could therefore plot the integral of the difference spectrum against the ligand fraction, and determine K_D by fitting

$$I([L]) = I_0[PL] = I_0 \frac{[P]_{\text{tot}}[L]_{\text{tot}}}{[L]_{\text{tot}} + K_D} \tag{4.16}$$

However, the free ligands will also repolarize with their T_1. Once the repolarization due to T_1 balances the depolarization due to the saturation, saturating for longer time will not change the ligand signal anymore. If we plot the integral of the difference spectrum (green spectrum in Fig. 4.3) as a function of the duration of the saturation pulse, we therefore obtain a curve that first grows linearly, and then reaches a plateau at a fixed value.

Corresponding data are shown for five different concentrations in Fig. 4.4. The data may be modelled using the following function:

$$I(\tau) = a(1 - \exp(-b\tau)) \tag{4.17}$$

The most quantitative measure of [PL] is not the difference integral for a fixed transfer time, but rather the *growth of that integral for short pulse durations* τ. But this growth is exactly the derivative of $I(\tau)$ at $t = 0$. For lack of a better name, it is referred to in the literature as amplification factor:

$$\alpha_0 = \left.\frac{\partial I(\tau)}{\partial \tau}\right|_{\tau=0} = ab \tag{4.18}$$

We therefore determine a and b from every curve in Fig. 4.4, and plot the product $\alpha_0 = ab$ against the ligand concentration $[L]$. These data are

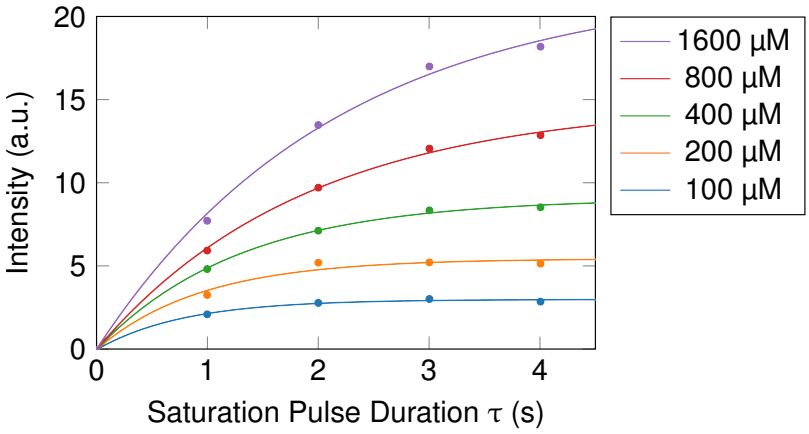

Figure 4.4: Integral of the difference spectrum as function of the saturation pulse for different ligand concentrations. The solid lines show fits according to Eq. (4.17).

then fitted with our well-known expression for $[PL]$:

$$\alpha_0 = \alpha_0' \frac{[P]_{\text{tot}}[L]_{\text{tot}}}{[L]_{\text{tot}} + K_D} \tag{4.19}$$

The experimental data and the fit are shown in Fig. 4.5. The obtained value for K_D is 190 µM. Notwithstanding a proper error analysis, we can estimate the accuracy of this measurement to be no better than 10 %.

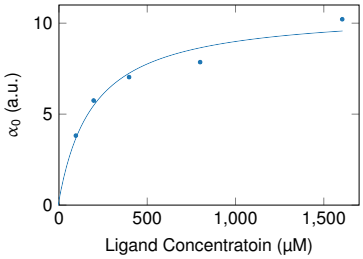

Figure 4.5: Plot of the amplificaiton factor for different concentrations, along with a fit according to Eq. (4.19).

4.8 The water-LOGSY Experiment

The waterLOGSY experiment is an alternative experiment for the detection of binding of small molecules to proteins. We will again use the trytophan / BSA system, so that the samples are identical to the ones we used for the STD experiment.

However, rather than saturating the protein and looking at the difference this does to the NMR spectra, we now look at the difference of the spectrum when we (a) apply RF power outside the NMR spectrum and (b) saturate the ^{1}H resonance of the water molecules. Again, at first sight, the two spectra would look identical. The spectrometer therefore records both spectra but saves only the difference. The resulting difference spectra are shown for various ligand concentrations in Fig. 4.6.

For small ligand concentrations, a significant fraction of the ligand is bound to the protein, and saturation of the water resonance leads to a Nuclear Overhauser Effect of large molecules, which has a negative sign. Hence the on-resonance irradiated spectrum is a bit smaller, and when computing the difference, we obtain a positive signal.

As the ligand concentration is increased, the NOE for small molecules dominates, which has a positive sign. Hence, the on-resonance irradiated spectrum is a bit larger, and when computing the difference, we obtain a negative signal.

A plot of the NOE signal, taken to be the spectral integral from 7.44 to 7.48 ppm is shown in Fig. 4.7. We may model the data with an expression that

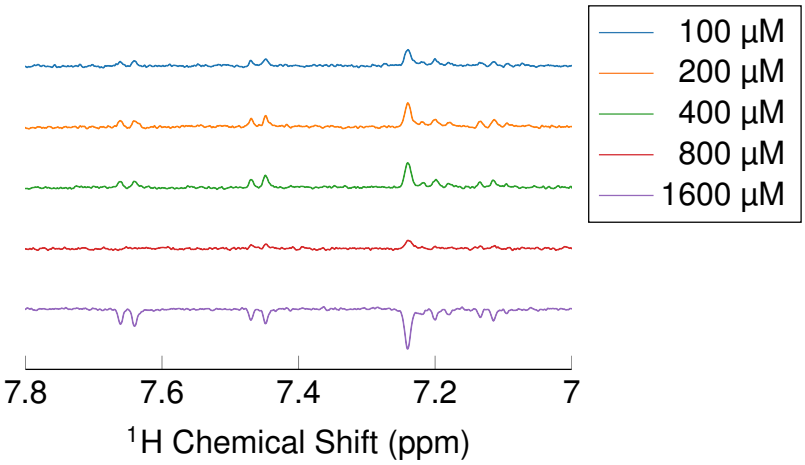

Figure 4.6: Aromatic part of spectra of a Tryptophan / BSA mixture (bottom orange) in buffer solution. The spectra only show signal intensity due to the water-based NOE. For small ligand concentrations, the NOE signal is dominated by contributions from ligands that are bound to the protein, i.e. by large molecules. As the concentration of the ligand is increased, eventually the NOE signal is dominated by contributions from free ligands, i.e., by small molecules, leading to a change in sign.

gives a positive contribution for the complex, and a negative contribution for the free ligand:

$$\eta_{\mathrm{WL}} = a[PL] - b[L] \tag{4.20}$$

$$= a\frac{[P]_{\mathrm{tot}}[L]_{\mathrm{tot}}}{[L]_{\mathrm{tot}} + K_D} - b[L], \tag{4.21}$$

where we have inserted our well-known expression for [PL] in the limit of a ligand excess.

The solid line in Fig. 4.7 is obtained from a non-linear regression, yielding a K_D value of 230 µM, in reasonable agreement with the value obtained from the STD analysis (190 µM).

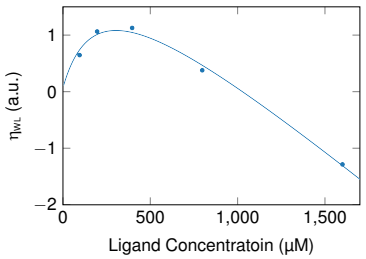

Figure 4.7: Plot of the waterLOGSY intensities η_{WL} for different concentrations, along with a fit according to Eq. (**??**).

4.9 Concluding Remarks

We have seen two different methods, saturation transfer difference and waterLOGSY, that can be used to detect ligand binding without hyperpolarization. In the STD experiment, we have taken care to observe the effect of the binding in the limit of a vanishing duration of the saturation pulse. However, we have taken no such precautions for the waterLOGSY experiment. We provisionally attribute the differences in our experimental protocols to this inconsistency.[2]

Note that careful data processing of the NMR spectra is required to obtain accurate results. For example, NMR spectra often exhibit a non-zero bsaeline, which would bias all the integrals, and cause substantial errors for the determination of K_D.

The STD experiment is readily extended to hyperpolarized spin systems. One can then work with much smaller ligand concentration, smaller protein concentration, and the exact expression for $[PL]$. It should be noted, that the STD experiment works well only with protons. One therefore has to work with ligands with hyperpolarized protons, and detect the spectrum in relatively short time.

The waterLOGSY experiment may likewise be combined with hyperpolarization. We have already observed 1H enhancement son water of the order of 300. These will, correspondingly, give a 300-fold larger

2: It will be the privilege of next year's students to study waterLOGSY in the limit of a vanishing saturation pulse length.

Overhauser effect, and hence again reduce the required amount of ligand and protein.

4.10 Further Reading

- To read more about NMR based drug screening, have a look at the review written by Alvar Gossert and Wolfgang Jahnke [15].

Bibliography

References in citation order.

[1] Albert W. Overhauser. 'Polarization of Nuclei in Metals'. In: *Phys. Rev.* 92.2 (1953), pp. 411–415. DOI: 10.1103/physrev.92.411 (cited on pages 6, 24).

[2] T. R. Carver and C. P. Slichter. 'Polarization of Nuclear Spins in Metals'. In: *Physical Review* 92.1 (1953), pp. 212–213. DOI: 10.1103/physrev.92.212.2 (cited on pages 6, 24).

[3] Charles P. Slichter. 'The Discovery and Demonstration of Dynamic Nuclear Polarization-A Personal and Historical Account'. In: *Physical Chemistry Chemical Physics* 12.22 (2010), p. 5741. DOI: 10.1039/c003286g (cited on pages 7, 24).

[4] Matthew L. Hirsch et al. 'Brute-Force Hyperpolarization for NMR and MRI'. In: *Journal of the American Chemical Society* 137.26 (2015), pp. 8428–8434. DOI: 10.1021/jacs.5b01252 (cited on page 7).

[5] D.I Hoult and R.E Richards. 'The Signal-To-Noise Ratio of the Nuclear Magnetic Resonance Experiment'. In: *Journal of Magnetic Resonance (1969)* 24.1 (1976), pp. 71–85. DOI: 10.1016/0022-2364(76)90233-x (cited on page 10).

[6] Charles P. Slichter. 'Principles of Magnetic Resonance'. In: *Springer Series in Solid-State Sciences* (1990). DOI: 10.1007/978-3-662-09441-9 (cited on page 11).

[7] F.D Doty et al. 'Noise in High-Power, High-Frequency Double-Tuned Probes'. In: *Journal of Magnetic Resonance (1969)* 77.3 (1988), pp. 536–549. DOI: 10.1016/0022-2364(88)90011-x (cited on page 12).

[8] H. Nyquist. 'Thermal Agitation of Electric Charge in Conductors'. In: *Physical Review* 32.1 (1928), pp. 110–113. DOI: 10.1103/physrev.32.110 (cited on page 12).

[9] Helena Kovacs, Detlef Moskau, and Manfred Spraul. 'Cryogenically Cooled Probes-A Leap in NMR Technology'. In: *Progress in Nuclear Magnetic Resonance Spectroscopy* 46.2-3 (2005), pp. 131–155. DOI: 10.1016/j.pnmrs.2005.03.001 (cited on page 12).

[10] Ēriks Kupče et al. 'Parallel Nuclear Magnetic Resonance Spectroscopy'. In: *Nature Reviews Methods Primers* 1.1 (2021), p. 27. DOI: 10.1038/s43586-021-00024-3 (cited on page 13).

[11] Malcolm H. Levitt. 'Spin Dynamics: Basics of Nuclear Magnetic Resonance'. In: (2008) (cited on pages 13, 21).

[12] Nate Silver. *The Signal and the Noise: Why So Many Predictions Fail-But Some Don't*. Penguin Press, 2013 (cited on page 13).

[13] Jozef Kowalewski and Lena Mäler. *Nuclear Spin Relaxation in Liquids*. Series in Chemical Physics. Taylor & Francis, 2006, nil (cited on page 20).

[14] C. D. Jeffries. 'Polarization of Nuclei By Resonance Saturation in Paramagnetic Crystals'. In: *Phys. Rev.* 106.1 (1957), pp. 164–165. DOI: 10.1103/physrev.106.164 (cited on page 27).

[15] Alvar D. Gossert and Wolfgang Jahnke. 'Nmr in Drug Discovery: A Practical Guide To Identification and Validation of Ligands Interacting With Biological Macromolecules'. In: *Progress in Nuclear Magnetic Resonance Spectroscopy* 97.nil (2016), pp. 82–125. DOI: 10.1016/j.pnmrs.2016.09.001 (cited on pages 31, 38).